© 2002 The Chemical Society of Japan

Synthesis and Magnetic Properties of $Mn^{III}Mn^{II}Mn^{III}$ Trinuclear Complexes with Hydroxo Bridges. Comparison of Magnetic Properties between Hydroxo- and Alkoxo-Bridged Complexes by Density Functional Calculations

Masakazu Hirotsu,* Mutsumi Aoyagi,† Masaaki Kojima,†† Wasuke Mori,††† and Yuzo Yoshikawa††

Department of Chemistry, Faculty of Engineering, Gunma University, Kiryu, Gunma 376-8515

†Institute for Molecular Science, Okazaki, Aichi 444-8585

††Department of Chemistry, Faculty of Science, Okayama University, Tsushima, Okayama 700-8530

†††Department of Chemistry, Faculty of Science, Kanagawa University, 2946 Tsuchiya, Hiratsuka, Kanagawa 259-1293

(Received May 31, 2001)

A hydroxo-bridged $Mn^{III}Mn^{II}Mn^{III}$ trinuclear complex, $[Mn_3(L^1)_2(2,6\text{-dcba})_2(OH)_2]$ (**1**), where H_2L^1 is *N*,*N*-bis-(2-hydroxybenzyl)-*N*′,*N*′-dimethylethylenediamine and H2,6-dcba is 2,6-dichlorobenzoic acid, was synthesized by the reaction of $Mn(ClO_4)_2{\cdot}6H_2O$ with H_2L^1, H2,6-dcba, and a base in acetonitrile. The structure of **1** was determined by X-ray crystallography: **1** crystallizes in the monoclinic space group $P2_1/c$ with $a = 9.616(4)$ Å, $b = 12.537(4)$ Å, $c = 23.099(4)$ Å, $\beta = 94.73(2)°$, $V = 2775(1)$ Å^3, and $Z = 2$. The central Mn^{II} and terminal Mn^{III} ions are bridged by phenolato, carboxylato, and hydroxo ligands to form a linear Mn^{III}–Mn^{II}–Mn^{III} arrangement. The bridging structure between Mn^{III} and Mn^{II} is similar to that of analogous alkoxo-bridged complexes, $[Mn_3(L)_2(\text{carboxylato})_2(\text{alkoxo})_2]$, where L is L^1 or its derivatives. Most of the alkoxo-bridged complexes $[Mn_3(L)_2(\text{carboxylato})_2(\text{alkoxo})_2]$ exhibit a weak ferromagnetic interaction between Mn^{III} and Mn^{II}, while the hydroxo-bridged complex **1** exhibits a weak antiferromagnetic interaction. A comparison of the magnetic properties between the hydroxo- and alkoxo-bridged complexes was performed by density functional calculations of $Mn^{III}Mn^{II}$ dinuclear model complexes.

Multinuclear manganese centers play an important role in biochemistry related to redox enzymes.[1–5] Dinuclear manganese sites have been found in catalases, alginases, and ribonucleotide reductases.[2] In the oxygen-evolving complex of photosystem II, a tetranuclear manganese cluster acts as an active site for photosynthetic water oxidation in which the four-electron redox reaction proceeds stepwise via five characteristic oxidation states, from S_0 to S_4.[3–5] Efforts to prepare model complexes have provided diverse bridging structures consisting of oxo, carboxylato, phenolato, and other O donating ligands; their spectroscopic and magnetic properties have been extensively studied. The correlations between the magnetic property and the bridging structure have become apparent experimentally. From a theoretical viewpoint, the electronic structures and the Heisenberg spin-coupling parameters (J) of oxo-bridged dinuclear manganese complexes have been calculated.[6–9] It has been suggested that the Heisenberg J parameters calculated using density functional methods combined with the broken symmetry and spin projection concepts well correspond to the experimental J values. Recently, we have synthesized $Mn^{III}Mn^{II}Mn^{III}$ trinuclear complexes, $[Mn_3(L)_2(\text{carboxylato})_2(\text{alkoxo})_2]$, where L represents the tripodal tetradentate ligand (Fig. 1) and the Mn^{III} and Mn^{II} centers are bridged by alkoxo, phenolato, and carboxylato ligands.[10,11] Both ferromagnetic and antiferromagnetic super-exchange interactions,

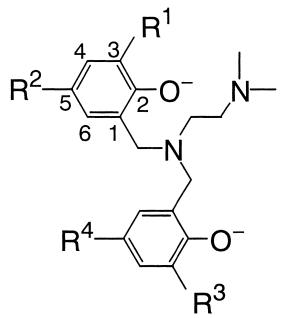

	R^1	R^2	R^3	R^4
L^1	H	H	H	H
L^2	*t*-Bu	*t*-Bu	H	H
L^3	*t*-Bu	*t*-Bu	*t*-Bu	*t*-Bu
L^4	H	OCH_3	H	OCH_3
L^5	*t*-Bu	*t*-Bu	OCH_3	H
L^6	H	H	OCH_3	H

Fig. 1. Tripodal tetradentate ligands.

which are weak, were observed. This was explained by considering the antiferromagnetic contribution of the carboxylato bridge and the ferromagnetic contribution of the phenolato and alkoxo bridges. However, the qualitative evaluation was difficult because of many exchange pathways. In such a case, the theoretical calculation of the *J* parameter is very effective.

In this paper, we report the synthesis, structure, and magnetic properties of the hydroxo-bridged $Mn^{III}Mn^{II}Mn^{III}$ trinuclear complex $[Mn_3(L^1)_2(2,6\text{-dcba})_2(OH)_2]$ (**1**). The spin-exchange interaction between Mn^{II} and Mn^{III} is antiferromagnetic, which is different from the ferromagnetic interaction observed for most of the alkoxo-bridged complexes $[Mn_3(L)_2(carboxylato)_2(alkoxo)_2]$. The relationship between the bridging ligands (OH and OCH_3) and the magnetic properties was examined by performing density functional calculations of $Mn^{III}Mn^{II}$ dinuclear models.

Experimental

Abbreviations. The tripodal tetradentate ligands used in this text are illustrated in Fig. 1. The abbreviations of carboxylic acid are as follows: Hba = benzoic acid, Hmcba = *m*-chlorobenzoic acid, H2,6-dcba = 2,6-dichlorobenzoic acid, H3,5-dcba = 3,5-dichlorobenzoic acid, Hpmba = *p*-methoxybenzoic acid, and Hbf = benzoylformic acid.

$[Mn_3(L^1)_2(2,6\text{-dcba})_2(OH)_2]$ (1). The tripodal ligand H_2L^1 was prepared according to a literature procedure.[10,12] To a solution containing $Mn(ClO_4)_2{\cdot}6H_2O$ (0.380 g, 1.05 mmol) in acetonitrile (10 cm^3) were added H_2L^1 (0.210 g, 0.7 mmol), H2,6-dcba (0.134 g, 0.7 mmol), and *N*,*N*-diisopropylethylamine (0.476 cm^3, 2.8 mmol). The dark brown solution was stirred at room temperature for 3 h. The resulting dark green precipitate was collected by filtration and washed with acetonitrile. The product was dissolved in dichloromethane (10 cm^3) and filtered. To the filtrate was added acetonitrile (10 cm^3); this solution was allowed to stand at room temperature. Black prismatic crystals were deposited, collected by filtration, washed with acetonitrile, and dried over P_4O_{10} under vacuum. Yield: 0.307 g (75%). Found: C, 50.43; H, 4.36; N, 5.06%. Calcd for $C_{50}H_{52}Cl_4Mn_3N_4O_{10}$: C, 51.08; H, 4.46; N, 4.77%. IR (KBr pellet) ν_{as}(COO) 1596, ν_s(COO) 1389 cm^{-1}. μ_{eff} (294 K) 8.71 μ_B. A piece of the crystal was used for the X-ray crystal structure determination.

The preparation of $[Mn_3(L^2)_2(ba)_2(OH)_2]$ (**2**) has been reported in the preceding paper.[11]

$[Mn_3(L^1)_2(3,5\text{-dcba})_2(OCH_3)_2]{\cdot}2CH_2Cl_2$ (3). To a solution containing $Mn(ClO_4)_2{\cdot}6H_2O$ (0.271 g, 0.75 mmol) in methanol (10 cm^3) were added H_2L^1 (0.150 g, 0.5 mmol), H3,5-dcba (0.096 g, 0.5 mmol), and *N*,*N*-diisopropylethylamine (0.340 cm^3, 2.0 mmol). The dark brown solution was stirred at room temperature for 3 h. The resulting dark green precipitate was collected by filtration and washed with methanol. The product was dissolved in dichloromethane (20 cm^3) and filtered. To the filtrate was added methanol (10 cm^3); this solution was allowed to stand at room temperature. Dark green crystals were deposited, collected by filtration, washed with methanol, and dried over P_4O_{10} under vacuum. Yield: 0.284 g (83%). Found: C, 46.97; H, 4.27; N, 4.17%. Calcd for $C_{54}H_{60}Cl_8Mn_3N_4O_{10}$: C, 47.22; H, 4.40; N, 4.08%. IR (KBr pellet) ν_{as}(COO) 1598, ν_s(COO) 1377 cm^{-1}. μ_{eff} (293 K) 9.30 μ_B.

Physical Measurements. Infrared spectra were recorded with a JASCO IR-810 spectrophotometer. Magnetic susceptibility data in the 2–300 K temperature range were collected using a Quantum Design MPMS-5S SQUID magnetometer. The applied magnetic field was 1 T for **1** and **2**, and 0.1 T for **3**. Room-temperature magnetic susceptibilities were measured with a Sherwood Scientific Ltd., Model MK1 magnetic susceptibility balance. The susceptibilities were corrected for diamagnetism estimated from Pascal's constants. Elemental analyses were carried out on a Perkin Elmer 2400 II elemental analyzer.

Crystal Structure Determination. A black prismatic crystal of **1** (0.45 × 0.25 × 0.45 mm) was mounted on a glass fiber. Diffraction measurements were made on a Rigaku AFC-5R diffractometer at the X-ray Laboratory of Okayama University using graphite-monochromated Mo $K\alpha$ radiation. Crystallographic data are summarized in Table 1. The cell parameters were obtained by a least-squares refinement of the angular settings of 25 reflections in the range $24° < 2\theta < 25°$. The intensity data were collected by the ω-2θ scan technique to a maximum 2θ value of 52°. The intensities of three standard reflections were measured after every 97 reflections and showed no significant reduction during the data collection. An empirical absorption correction based on ψ scans of three reflections was applied. All calculations were carried out using the teXsan crystallographic software package.[13] The structure was solved by direct methods and expanded using Fourier techniques. All non-hydrogen atoms were refined anisotropically by a full-matrix least-squares procedure. Hydrogen atoms were placed at fixed distances from bonded carbon atoms of 0.95 Å and included in the model but not refined, except for H26(hydroxo) which was refined isotropically. The maximum and minimum peaks on the final difference Fourier map corresponded to 0.63 and −0.67 e $Å^{-3}$, respectively.

Lists of the final atomic coordinates and thermal factors and of complete bond distances and angles, and a fully labeled ORTEP diagram have been deposited as Document No. 75010 at the Office of the Editor of Bull. Chem. Soc. Jpn. Crystallographic data have been deposited at the CCDC, 12 Union Road, Cambridge CB2 1EZ, UK and copies can be obtained on request, free of charge, by quoting the publication citation and the deposition number CCDC 174542.

Computational Details. Quantum chemical calculations were performed with the Gaussian 94 program package.[14] The alkoxo-bridged $Mn^{III}Mn^{II}$ dinuclear complex used for the calcula-

Table 1. Crystallographic Data of $[Mn_3(L^1)_2(2,6\text{-dcba})_2(OH)_2]$ (**1**)

Empirical formula	$C_{50}H_{52}Cl_4Mn_3N_4O_{10}$
Fw	1175.59
Space group	$P2_1/c$ (No. 14)
a/Å	9.616(4)
b/Å	12.537(4)
c/Å	23.099(4)
β/deg	94.73(2)
V/$Å^3$	2775(1)
Z	2
T/K	298
Radiation λ/Å	0.7107
ρ_{calcd}/g cm^{-3}	1.407
μ(Mo $K\alpha$)/cm^{-1}	9.21
R[a)]	0.058
R_w[b)]	0.052

a) $R = \Sigma||F_o|-|F_c||/\Sigma|F_o|$.
b) $R_w = [\Sigma w(|F_o|-|F_c|)^2/\Sigma wF_o^2]^{1/2}$, $w = 1/\sigma^2(F_o)$.

tions was modeled on the structurally characterized complex $[Mn^{III}(L^5)(CH_3OH)(OCH_3)Mn^{II}Cl_2]$.[11] The hydroxo-bridged model was obtained by replacing OCH_3 with OH. Before density functional calculations, the structures of model complexes were optimized by using a molecular mechanics calculation program, MMP2 (1986), in which the Mn and coordinated atoms, and their adjacent atoms were fixed at the experimental coordinate of $[Mn^{III}(L^5)(CH_3OH)(OCH_3)Mn^{II}Cl_2]$. The H atom of the hydroxo bridging ligand was located on the O–C axis of the alkoxo bridging ligand, and three O–H bond distances (0.95, 1.00, and 1.05 Å) were used. The evaluation of spin-exchange parameters was performed by the broken symmetry method. The spin Hamiltonian of the mixed-valence $Mn^{III}Mn^{II}$ dinuclear model is given by

$$H = -2JS_1 \cdot S_2,$$

where J is the magnetic exchange parameter for the $S_1 = 2$, $S_2 = 5/2$ spin system. The high-spin state (HS) and the broken symmetry state (BS) were built according to a reference.[15] The resonance term was neglected, and the lowest high-spin state energy was used to calculate the J parameter. The energy difference between the high-spin and broken symmetry states is given by

$$E_{HS} - E_{BS} = -4JS_1S_2,$$

where E_{HS} and E_{BS} were obtained by density functional calculations.

Results and Discussion

Structure of $[Mn_3(L^1)_2(2,6\text{-dcba})_2(OH)_2]$ (1). The molecular structure of the $Mn^{III}Mn^{II}Mn^{III}$ trinuclear complex **1** is shown in Fig. 2, and selected bond distances and angles are listed in Table 2. Three manganese ions are linearly arranged, and each of the two flanking Mn^{III} ions is surrounded by a tripodal tetradentate ligand, L^1. The central Mn^{II} ion is located on a crystallographic inversion center, and the asymmetric unit is a half-molecule of **1**. The Mn^{III} and Mn^{II} ions are bridged by the phenolato O donor from the L^1 ligand, the hydroxo O donor, and the carboxylato ligand. Such a bridging structure has been found for $[Mn_3(L)_2(\text{carboxylato})_2(OCH_3)_2]$, in which alkoxo bridges exist instead of the hydroxo bridges in **1**. As to the MnO_2Mn bridging structure associated with the hydroxo

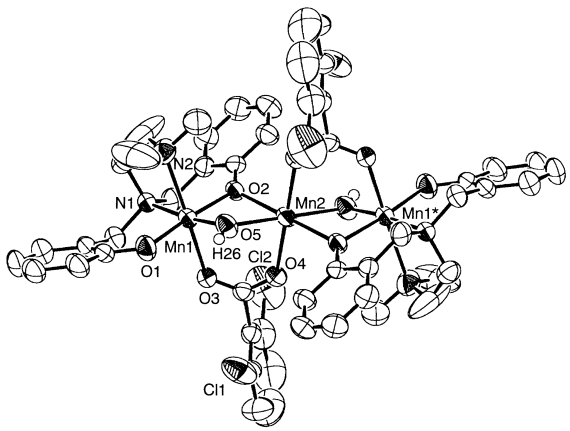

Fig. 2. A perspective view of $[Mn_3(L^1)_2(2,6\text{-dcba})_2(OH)_2]$ (**1**). Ellipsoids represent 50% probability.

Table 2. Selected Bond Distances (Å) and Angles (deg) of $[Mn_3(L^1)_2(2,6\text{-dcba})_2(OH)_2]$ (**1**)

Mn1–O1	1.866(4)	Mn1–N2	2.377(5)
Mn1–O2	1.920(3)	Mn2–O2	2.217(3)
Mn1–O3	2.266(4)	Mn2–O4	2.158(4)
Mn1–O5	1.892(4)	Mn2–O5	2.122(5)
Mn1–N1	2.090(4)	Mn1···Mn2	3.1236(8)
O1–Mn1–O2	174.1(1)	O3–Mn1–N2	169.4(2)
O1–Mn1–O3	90.7(1)	O5–Mn1–N1	173.6(2)
O1–Mn1–O5	91.3(2)	O5–Mn1–N2	94.4(2)
O1–Mn1–N1	92.9(2)	N1–Mn1–N2	80.7(2)
O1–Mn1–N2	93.9(2)		
O2–Mn1–O3	87.4(1)	O2–Mn2–O4	87.1(1)
O2–Mn1–O5	83.3(2)	O2–Mn2–O5	71.4(1)
O2–Mn1–N1	92.6(1)	O4–Mn2–O5	88.7(2)
O2–Mn1–N2	88.9(2)	Mn1–O2–Mn2	97.8(1)
O3–Mn1–O5	95.0(2)	Mn1–O5–Mn2	102.1(2)
O3–Mn1–N1	89.6(1)		

and phenolato ligands, the Mn1–O5(hydroxo)–Mn2 angle (102.1(2)°) is quite similar to the corresponding Mn^{III}–O(alkoxo)–Mn^{II} angles (average 102.4°) in $[Mn_3(L^1)_2(\text{mcba})_2(OCH_3)_2]$, $[Mn_3(L^2)_2(\text{mcba})_2(OCH_3)_2]$, and $[Mn_3(L^1)_2(\text{bf})_2(OCH_3)_2]$.[10] The Mn1–O2(phenolato)–Mn2 angle (97.8(1)°) is also similar to those of the alkoxo-bridged complexes (average 98.9°). The two MnO_2 planes in the Mn_2O_2 tetragon form a hinge angle of 157.52°, as found for $[Mn_3(L^1)_2(\text{mcba})_2(OCH_3)_2]$ (153.93°), $[Mn_3(L^2)_2(\text{mcba})_2(OCH_3)_2]$ (155.55°), and $[Mn_3(L^1)_2(\text{bf})_2(OCH_3)_2]$ (159.38 and 157.43°). The Mn1–O5(hydroxo), Mn1–O2(phenolato), and Mn2–O2(phenolato) distances (1.892(4), 1.920(3), and 2.217(3) Å, respectively) in **1** are similar to the corresponding Mn^{III}–O(alkoxo), Mn^{III}–O(phenolato), and Mn^{II}–O(phenolato) distances (1.900(2), 1.947(2), and 2.246(2) Å, respectively) in $[Mn_3(L^1)_2(\text{mcba})_2(OCH_3)_2]$, but the Mn2–O5(hydroxo) distance (2.122(5) Å) in **1** is smaller than the Mn^{II}–O(alkoxo) distance (2.180(2) Å) in $[Mn_3(L^1)_2(\text{mcba})_2(OCH_3)_2]$. As a result, the $Mn^{III}\cdots Mn^{II}$ separation of $[Mn_3(L^1)_2(2,6\text{-dcba})_2(OH)_2]$ (3.1236(8) Å) is slightly smaller than that of $[Mn_3(L^1)_2(\text{mcba})_2(OCH_3)_2]$ (3.1720(7) Å).[10] In structurally characterized $Mn^{III}Mn^{II}Mn^{III}$ or $Mn^{II}Mn^{III}$-Mn^{II} complexes with hydroxo bridges, the Mn^{III}–O(hydroxo) distances are in the range of 1.840–1.850 Å, and the Mn^{II}–O(hydroxo) distances range from 1.980 to 2.138 Å.[16,17] In **1**, the corresponding Mn^{III}–O(hydroxo) distance is larger, while the Mn^{II}–O(hydroxo) distance is located at the upper limit of the normal range. This indicates that the Mn–O(hydroxo) distances are affected by the other bridging ligands. Therefore, the bridging structures of $[Mn_3(L)_2(\text{carboxylato})_2(OH)_2]$ and $[Mn_3(L)_2(\text{carboxylato})_2(\text{alkoxo})_2]$ could be regarded as comparable.

Synthesis. The reaction of $Mn(ClO_4)_2 \cdot 6H_2O$ (1.5 equiv) with H_2L^1 (1 equiv), 2,6-dichlorobenzoic acid (2 equiv), and *N*,*N*-diisopropylethylamine (4 equiv) in acetonitrile gave an $Mn^{III}Mn^{II}Mn^{III}$ trinuclear complex containing hydroxo bridges, $[Mn_3(L^1)_2(2,6\text{-dcba})_2(OH)_2]$ (**1**). When benzoic acid was used instead of 2,6-dcba, an $Mn^{III}Mn^{II}Mn^{III}$ trinuclear complex including four carboxylato bridges, $[Mn_3(L^1)_2(\text{ba})_4]$, has been obtained.[11] This indicates that the chloro groups on 2,6-dcba

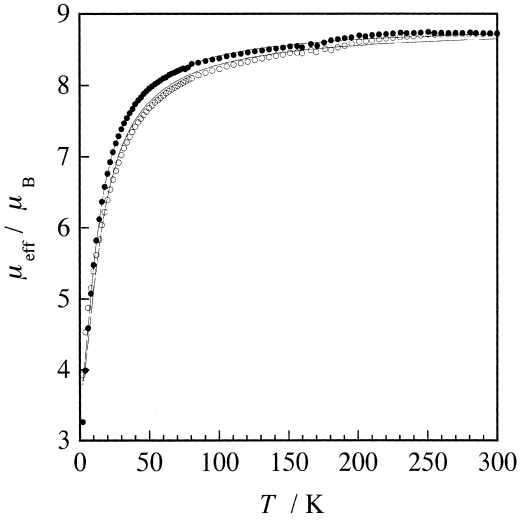

Fig. 3. Temperature dependence of the magnetic moments per molecule of **1** (○) and **2** (●). Solid lines represent the least-squares fit.

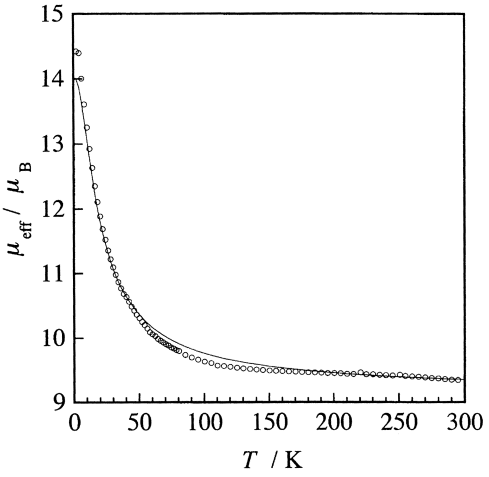

Fig. 4. Temperature dependence of the magnetic moments per molecule of **3** (○). A solid line represents the least-squares fit.

are important for the formation of the hydroxo bridge in **1**. On the other hand, the reaction using H_2L^2 and benzoic acid has produced an analogous hydroxo-bridged trinuclear complex, $[Mn_3(L^2)_2(ba)_2(OH)_2]$ (**2**). A trinuclear complex with four carboxylato bridges, such as $[Mn_3(L^2)_2(ba)_4]$, could not form because of the large steric interaction between the 3-positioned *t*-butyl group on the L^2 ligand and the additional carboxylato ligand. If the L^1 ligand and 2,6-dcba form an $Mn^{III}Mn^{II}Mn^{III}$ trinuclear complex with four carboxylato bridges, $[Mn_3(L^1)_2(2,6\text{-dcba})_4]$, a large steric repulsion would be exerted by the chloro groups on 2,6-dcba. Consequently, the sterically hindered ligands selectively construct the hydroxo-bridged $Mn^{III}Mn^{II}Mn^{III}$ trinuclear structures of **1** and **2**. An alkoxo-bridged $Mn^{III}Mn^{II}Mn^{III}$ trinuclear complex, $[Mn_3(L^1)_2(3,5\text{-dcba})_2(OCH_3)_2]\cdot 2CH_2Cl_2$ (**3**), was also prepared in order to examine the substituent effect of the carboxylato bridging ligand on the magnetic property of $[Mn_3(L^1)_2(\text{carboxylato})_2(\text{alkoxo})_2]$.

Magnetic Properties. Temperature-dependent magnetic susceptibility data of **1**, **2**, and **3** were measured in the 2–300 K temperature range. The results are plotted in Figs. 3 and 4 as μ_{eff} vs T. The effective magnetic moments decrease from 8.72 μ_B at 300 K to 3.93 μ_B at 2 K for **1** and from 8.74 μ_B at 300 K to 3.26 μ_B at 2 K for **2**. These data indicate that the manganese ions interact antiferromagnetically. On the other hand, the effective magnetic moment of **3** increases from 8.74 μ_B at 300 K to 14.42 μ_B at 2 K, indicating a ferromagnetic interaction.

The Heissenberg Hamiltonian in the isotropic spin exchange coupling model is given by

$$H = -2[J_{12}S_1\cdot S_2 + J_{23}S_2\cdot S_3 + J_{13}S_1\cdot S_3],$$

where $S_1 = S_3 = 2$ and $S_2 = 5/2$ for the S_1–S_2–S_3 arrangement. As shown in the structure of **1**, the terminal Mn^{III} ions in the $Mn^{III}Mn^{II}Mn^{III}$ complexes are in an equivalent environment. Therefore, the spin-exchange interaction between Mn^{III} and Mn^{II} is designated as $J = J_{12} = J_{23}$. The terminal interaction between the Mn^{III} ions can be excluded because of the large $Mn^{III}\cdots Mn^{III}$ separation ($J_{13} = 0$). A theoretical expression for the molar magnetic susceptibility is derived using the Kambe vector-coupling method and the Van Vleck equation. For $Mn^{III}Mn^{II}Mn^{III}$ trinuclear complexes, other authors have assumed different g values for Mn^{III} and Mn^{II} in the Zeeman Hamiltonian, while the use of isotropic g values also gives satisfactory results.[18,19] The latter model was adopted here. Least-squares fits of the data were made for two parameters, J and g, and are represented by the solid lines in Figs. 3 and 4. The minimized function was $\Sigma[(\mu_{eff})_{exptl}-(\mu_{eff})_{calcd}]^2$. The obtained parameters are as follows: $J = -1.26$ cm^{-1}, $g = 1.94$ for **1**; $J = -1.07$ cm^{-1}, $g = 1.95$ for **2**; $J = 1.43$ cm^{-1}, $g = 2.00$ for **3**.

The magnetic properties of **1**, **2**, and **3** are summarized in Table 3 together with those of related mixed-valence manganese complexes. The bridging structures between Mn^{III} and Mn^{II} are illustrated in Fig. 5. The alkoxo-bridged complex, $[Mn_3(L)_2(\text{carboxylato})_2(\text{alkoxo})_2]$ (type A), is almost isostructural to the hydroxo-bridged complex, $[Mn_3(L)_2(\text{carboxylato})_2(OH)_2]$ (type D); the magnetic properties nevertheless differ from each other. The magnetic interaction in the hydroxo-bridged complexes of type D is antiferromagnetic, while most of the alkoxo-bridged complexes, types A and B, exhibit ferromagnetic interactions.

Geometry Optimization of a Mononuclear Manganese(III) Complex. In order to evaluate the validity of the computational method, the geometry of a model complex, $[Mn(L^1)(ba)(CH_3OH)]$, was optimized by quantum chemical calculations; the calculated structure is shown in Fig. 6. An analogous complex, $[Mn(L^3)(mcba)(CH_3OH)]$, has already been structurally characterized by X-ray analysis.[10] The distances of the coordination bonds in the optimized structure of $[Mn(L^1)(ba)(CH_3OH)]$ and the experimental data from the X-ray analysis for $[Mn(L^3)(mcba)(CH_3OH)]$ are listed in Table 4.

First, the calculation was performed by the Hartree-Fock (HF) method using the LanL2MB basis set. In the Hartree-Fock method, the Mn(1)–O(3) distance is larger than that of Mn(1)–O(2) by 0.323 Å, which differs from the experimental results. The spin densities are 2.94 for Mn(1), −0.01 for O(2),

Table 3. Magnetic Properties of Polynuclear Manganese Complexes

Complex	Bridging structure	J / cm^{-1}	g	Ref.
$[Mn_3(L^1)_2(ba)_2(OCH_3)_2]$	A	1.05	1.98	10
$[Mn_3(L^1)_2(3,5\text{-dcba})_2(OCH_3)_2]$	A	1.43	2.00	this work
$[Mn_3(L^1)_2(mcba)_2(OC_2H_5)_2]$	A	0.65	1.99	11
$[Mn_3(L^2)_2(ba)_2(OCH_3)_2]$	A	1.9	2.00	10
$[Mn_3(L^2)_2(mcba)_2(OCH_3)_2]$	A	1.9	2.06	10
$[Mn_3(L^4)_2(pmba)_2(OCH_3)_2]$	A	−0.25	1.95	10
$[Mn(L^5)(OCH_3)(CH_3OH)MnCl_2]$	B	3.02	2.04	11
$[Mn_3(L^1)_2(ba)_4]$	C	−3.35	2.02	11
$[Mn_3(L^1)_2(2,6\text{-dcba})_2(OH)_2]$	D	−1.26	1.94	this work
$[Mn_3(L^2)_2(ba)_2(OH)_2]$	D	−1.07	1.95	this work

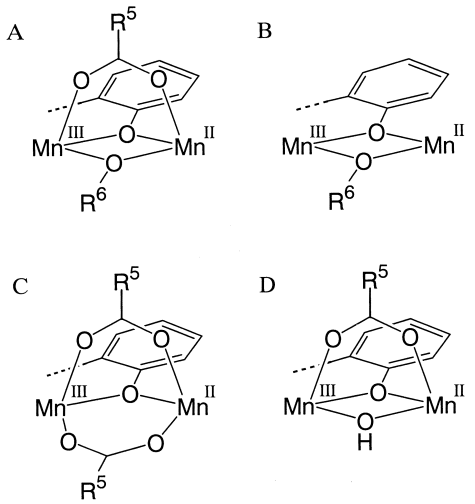

Fig. 5. Bridging structures between Mn^{III} and Mn^{II}. R^5COO and R^6O represent carboxylato and alkoxo ligands, respectively.

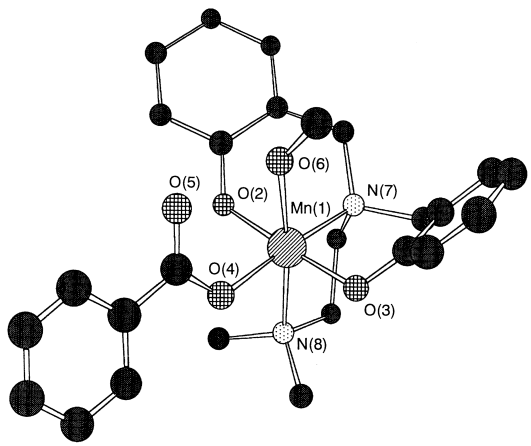

Fig. 6. The optimized structure of the Mn^{III} mononuclear model, $[Mn(L^1)(ba)(CH_3OH)]$.

and 1.04 for O(3). This implies that O(3) has a character of a phenoxy radical. On the other hand, the density functional calculation (B3LYP) using the same basis set (LanL2MB) gave different results. The bond distances of Mn(1)–O(2) and Mn(1)–O(3) are almost the same, and the spin densities are 3.18 for Mn(1), 0.21 for O(2), and 0.21 for O(3). These results

Table 4. Comparison of Optimized Geometry of $[Mn(L^1)(ba)(CH_3OH)]$ and Experimental Geometry of $[Mn(L^3)(mcba)(CH_3OH)]$ on Bond Length (Å)

Bond	UHF LanL2MB	UB3LYP LanL2MB	UB3LYP LanL2DZ	Experimental
Mn(1)–O(2)	1.812	1.792	1.873	1.865(3)
Mn(1)–O(3)	2.135	1.795	1.891	1.896(3)
Mn(1)–O(4)	1.914	1.914	2.022	1.999(3)
Mn(1)–O(6)	2.195	2.130	2.225	2.268(3)
Mn(1)–N(7)	2.145	2.188	2.186	2.098(3)
Mn(1)–N(8)	2.386	2.398	2.340	2.355(4)
O(5)···O(6)	2.377	2.401	2.538	2.597(5)

are more reasonable than the Hartree-Fock method, but the coordination bond distances deviate from the experimental data. The bond distances were improved by introducing the LanL2DZ basis set. The largest deviation is 0.09 Å for the Mn(1)–N(7) bond; the other distances are very similar to the experimental data. Therefore, we calculated the spin-exchange interactions using the density functional method (B3LYP) with the LanL2DZ basis set.

Evaluation of Spin-Exchange Interaction. As summarized in Table 3, most of the alkoxo-bridged complexes, types A and B, show ferromagnetic interactions. On the other hand, the hydroxo-bridged complexes studied here (type D) and the carboxylato-bridged complexes (type C) show antiferromagnetic interactions. However, the energy differences in the spin-exchange interactions between types A and D are very small, so it is difficult to discuss the magnetic exchange pathways through the alkoxo and hydroxo bridges. We therefore tried to calculate the energy of the spin-exchange interaction using quantum chemical methods. Because the $Mn^{III}Mn^{II}Mn^{III}$ trinuclear complex is too large for calculations, a dinuclear complex, $[Mn(L^5)(CH_3OH)(OCH_3)MnCl_2]$, was selected as a model compound containing an alkoxo-bridged $Mn^{III}Mn^{II}$ structure. For the $Mn^{III}Mn^{II}Mn^{III}$ complexes with hydroxo bridges, a hydroxo-bridged $Mn^{III}Mn^{II}$ dinuclear model was used: the alkoxo bridging ligand in $[Mn(L^5)(CH_3OH)(OCH_3)MnCl_2]$ was replaced by a hydroxo bridge.

Figure 7 shows the structure of the alkoxo-bridged $Mn^{III}Mn^{II}$ dinuclear model complex used to calculate the spin-exchange interaction. In this model, the Mn and donor atoms and their adjacent atoms were fixed to the experimental positions from the X-ray crystal structure. The coordinates of the remaining atoms were optimized by a molecular mechanics calculation.

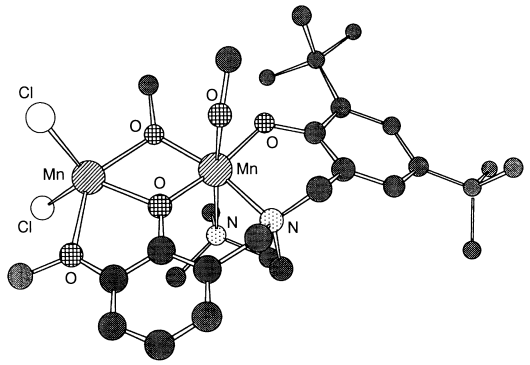

Fig. 7. The structure of the $Mn^{III}Mn^{II}$ dinuclear model, $[Mn(L^5)(CH_3OH)(OCH_3)MnCl_2]$.

Table 5. Calculated Values of Spin-Exchange Interactions between Mn^{III} and Mn^{II}

Model complex		J / cm^{-1}
$[Mn(L^5)(OCH_3)(CH_3OH)MnCl_2]$		14.01
$[Mn(L^6)(OCH_3)(CH_3OH)MnCl_2]$		15.20
$[Mn(L^5)(OH)(CH_3OH)MnCl_2]$	(O–H = 0.95 Å)	11.64
$[Mn(L^5)(OH)(CH_3OH)MnCl_2]$	(O–H = 1.00 Å)	12.36
$[Mn(L^5)(OH)(CH_3OH)MnCl_2]$	(O–H = 1.05 Å)	13.10

The density functional calculation of this dinuclear model led to a J value of 14.01 cm^{-1}, which indicates that the two manganese centers are ferromagnetically coupled (Table 5). This is consistent with the experimental results, because the experimental J value, 3.02 cm^{-1}, also shows a ferromagnetic interaction. However, the difference between the experimental and calculated values is large (ca. 11 cm^{-1}). To evaluate the substituent effect of the tripodal tetradentate ligand, we introduced a model complex, $[Mn(L^6)(CH_3OH)(OCH_3)MnCl_2]$: the two *t*-butyl groups are replaced by H atoms. The calculated J value is 15.20 cm^{-1}, which is larger than that for $[Mn(L^5)(CH_3OH)(OCH_3)MnCl_2]$ by 1.19 cm^{-1}. The difference is relatively small, and the substituent effect is not clearly recognized in the present experimental results.

The hydroxo-bridged model complex is $[Mn(L^5)(CH_3OH)(OH)MnCl_2]$, in which the atomic coordinates are identical to that of the alkoxo-bridged model, except for the hydroxo bridging ligand. The J values calculated for three O–H distances are 11.64 cm^{-1} for O–H = 0.95 Å, 12.36 cm^{-1} for O–H = 1.00 Å, and 13.10 cm^{-1} for O–H = 1.05 Å, indicating a ferromagnetic interaction between Mn^{III} and Mn^{II}. These results are distinct from the antiferromagnetic properties observed for the hydroxo-bridged $Mn^{III}Mn^{II}Mn^{III}$ complexes, **1** and **2**. The experimental J values for **1** and **2** are -1.26 and -1.07 cm^{-1}, respectively, which are smaller than the analogous alkoxo-bridged complexes by ca. 1–3 cm^{-1} (Table 3). The relative tendency in the experiment corresponds with the calculated results because the J values calculated for the hydroxo-bridged $Mn^{III}Mn^{II}$ dinuclear models are also smaller than that for the alkoxo-bridged one by 2.37 cm^{-1} (O–H = 0.95 Å), 1.65 cm^{-1} (O–H = 1.00 Å), and 0.91 cm^{-1} (O–H = 1.05 Å).

Consequently, although the calculated J values for the $Mn^{III}Mn^{II}$ dinuclear models include a large deviation, the relative tendency of analogous complexes can be estimated from these results. The ferromagnetic properties observed for the alkoxo-bridged $Mn^{III}Mn^{II}Mn^{III}$ complexes (type A) can be ascribed to that the ferromagnetic interactions through the alkoxo and phenolato bridges are comparable to, or larger than, the antiferromagnetic interaction through the carboxylato bridge. On the other hand, the weak antiferromagnetic property observed for the hydroxo-bridged $Mn^{III}Mn^{II}Mn^{III}$ complexes (type D) can be ascribed to that the ferromagnetic interactions through the hydroxo and phenolato bridges are smaller than the antiferromagnetic interaction through the carboxylato bridge. The reduction of the ferromagnetic interaction by 1–2 cm^{-1} for the hydroxo-bridged structure was suggested by the density functional calculations of the $Mn^{III}Mn^{II}$ dinuclear models.

References

1 V. L. Pecoraro, "Manganese Redox Enzymes," VCH, New York (1992).

2 G. C. Dismukes, *Chem. Rev.*, **96**, 2909 (1996).

3 V. K. Yachandra, K. Sauer, and M. P. Klein, *Chem. Rev.*, **96**, 2927 (1996).

4 C. Tommos and G. T. Babcock, *Acc. Chem. Res.*, **31**, 18 (1998).

5 A. Zouni, H.-T. Witt, J. Kern, P. Fromme, N. Krauβ, W. Saenger, and P. Orth, *Nature*, **409**, 739 (2001).

6 X. G. Zhao, W. H. Richardson, J.-L. Chen, J. Li, L. Noodleman, H.-L. Tsai, and D. N. Hendrickson, *Inorg. Chem.*, **36**, 1198 (1997).

7 J. E. McGrady and R. Stranger, *J. Am. Chem. Soc.*, **119**, 8512 (1997).

8 T. Soda, Y. Kitagawa, T. Onishi, Y. Takano, Y. Shigeta, H. Nagano, Y. Yoshioka, and K. Yamaguchi, *Chem. Phys. Lett.*, **319**, 223 (2000).

9 H. Nagao, M. Nishino, Y. Shigeta, T. Soda, Y. Kitagawa, T. Onishi, Y. Yoshioka, and K. Yamaguchi, *Coord. Chem. Rev.*, **198**, 265 (2000).

10 M. Hirotsu, M. Kojima, and Y. Yoshikawa, *Bull. Chem. Soc. Jpn.*, **70**, 649 (1997).

11 M. Hirotsu, M. Kojima, W. Mori, and Y. Yoshikawa, *Bull. Chem. Soc. Jpn.*, **71**, 2873 (1998).

12 C. J. Hinshaw, G. Peng, R. Singh, J. T. Spence, J. H. Enemark, M. Bruck, J. Kristofzski, S. L. Merbs, R. B. Ortega, and P. A. Wexler, *Inorg. Chem.*, **28**, 4483 (1989).

13 Crystal Structure Analysis Package, Molecular Structure Corporation, 1985 and 1992.

14 M. J. Frisch, G. W. Trucks, H. B. Schlegel, P. M. W. Gill, B. G. Johnson, M. A. Robb, J. R. Cheeseman, T. A. Keith, G. A. Petersson, J. A. Montgomery, K. Raghavachari, M. A. Al-Laham, V. G. Zakrzewski, J. V. Ortiz, J. B. Foresman, J. Cioslowski, B. B. Stefanov, A. Nanayakkara, M. Challacombe, C. Y. Peng, P. Y. Ayala, W. Chen, M. W. Wong, J. L. Andres, E. S. Replogle, R. Gomperts, R. L. Martin, D. J. Fox, J. S. Binkley, D. J. Defrees, J. Baker, J. P. Stewart, M. Head-Gordon, C. Gonzales, and J. A. Pople, "Gaussian 94, Rev E.1", Gaussian Inc., Pittsburgh, PA, 1995.

15 L. Noodleman, C. Y. Peng, D. A. Case, and J.-M. Mouesca, *Coord. Chem. Rev.*, **144**, 199 (1995), and references therein.

16 N. Kitajima, M. Osawa, S. Imai, K. Fujisawa, Y. Moro-oka, K. Heerwegh, C. A. Reed, and P. D. W. Boyd, *Inorg. Chem.*, **33**, 4613 (1994).

17 J.-C. Liu, Y. Xu, C.-Y. Duan, S.-L. Wang, F.-L. Liao, J.-Z. Zhuang, X.-Z. You, *Inorg. Chim. Acta*, **295**, 229 (1999).

18 D. P. Kessissoglou, M. L. Kirk, M. S. Lah, X. Li, C. Raptopoulou, W. E. Hatfield, and V. L. Pecoraro, *Inorg. Chem.*, **31**, 5424 (1992).

19 V. Tangoulis, D. A. Malamatari, K. Soulti, V. Stergiou, C. P. Raptopoulou, A. Terzis, T. A. Kabanos, and D. P. Kessissoglou, *Inorg. Chem.*, **35**, 4974 (1996).